Coverage Scalability Analysis of Multi-Cell LoRa Networks

Orestis Georgiou, Constantinos Psomas, and Ioannis Krikidis

Department of Electrical and Computer Engineering, University of Cyprus
email: last.firstname@ucy.ac.cy

***Abstract*— On the brink of the internet of things (IoT) revolution, different low power wide area network (LPWAN) technologies are competing for market share and scalability. In this paper we leverage stochastic geometry tools to better understand how one should model the uplink wireless coverage in a multi-cell LoRa network while taking under consideration both the effects of co-spreading factor interference and the spatial diversity afforded by the LoRa network server. To that end, we propose a tractable model that captures these two system peculiarities and mathematically show that gateway densification has an overall positive effect on network coverage thus supporting the scalability of LoRa networks.**

Keywords–LoRa, LPWAN, IoT, Coverage, Stochastic Geometry.

I. Introduction

The societal, environmental and industry benefits of the IoT are expected to be immense, enabling the remote monitoring, control of optimization of all sorts of intelligent processes [1]. Imperative to the success of this vision is the connectivity and affordability of wireless infrastructures. Low-power wide-area network (LPWAN) technologies facilitate to that effect [2] with LoRa [3] being a prime candidates among with others such as SigFox, Weightless, and Ingenu.

LoRa networks have been deployed in over 140 countries by both private and public operators. There have also been numerous academic studies on the performance of LoRA, notably towards improving its capacity, reliability and scalability [4]–[6]. For example, papers have proposed medium access control (MAC) protocol variations that can reduce the network's susceptibility to wireless interference [7]–[10].

One aspect that has not been adequately studied in the literature is the performance of multi-cell LoRa networks [9]. Namely, most papers have assumed that nearby LoRa gateways do not interact and thus are independent. This is an oversimplification that can lead to erroneously optimised protocols and incorrect conclusions about network scalability and capacity.

Our main contribution is that we propose a model that captures multi-gateway interactions as well as other interesting peculiarities of LoRa networks, as specified in Semtech whitepapers [3], [11]. We then demonstrate the tractability of this model by mathematically analysing the coverage and scalability of multi-cell LoRa networks. More specifically, we argue that multi-cell LoRa networks can be adequately approximated by appropriately thinned inhomogeneous Poisson point processes (PPPs). Then, leveraging tools from stochastic geometry [12], we obtain closed form expressions of various network properties such as the coverage probability, and use this to unveil the effects of gateway densification and how multiple gateways can help the network scale while maintaining adequate coverage.

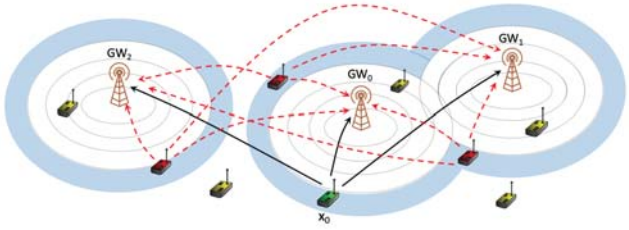

Fig. 1. System setup in the uplink of a multi-cell LoRa network.Three GWs, three interferers (red EDs), four non-interferes (yellow EDs) and one transmitting ED (green ED) are shown. The SF of the uplink transmission from the green ED $\mathbf{x}_0$ is decided by the distance d_{00} to its nearest GW_0. This uplink transmission may also be received by other GWs (GW_1 and GW_2) shown with black arrows. Transmitters that are within similar distances away from their respective GWs will by assigned the same SF as the green ED, and will interfere with each other's transmissions at all GWs. Interference links are shown using red dashed arrows. When two GWs are close to each other, tiers of SF will merge to form figure-eight zones.

II. Brief Introduction to LoRa

We provide here a very brief and by no means complete introduction to LoRa and its MAC layer called LoRaWAN. For further information, the reader is directed towards the Semtech white papers [3] and the LoRa Alliance specifications [3], [11], or to review papers like [2].

Most LoRa networks operate in the sub-GHz band with a maximum allowed transmit power of 14 and 21.7 dBm in Europe and the US, respectively. LoRa systems consist of end-devices (EDs), gateways (GW), and the NetServer (NS) forming a star of stars topology with the NS at the root, the GW at level one, and EDs as the leaves. At the heart of LoRa is a proprietary chirp spread spectrum (CSS) modulation scheme that supports adaptive data rates, thus enabling the system to trade-off throughput for coverage range, or robustness, or energy consumption, while keeping a constant bandwidth. This process is usually managed by the NS by regulating the bandwidth BW and the spreading factor $\text{SF} \in \{7, 8, \ldots, 12\}$ which determines the length of the chirp symbol $T_s = 2^{\text{SF}}/\text{BW}$. As such, the symbol duration and hence the time-on-air of a transmission increases exponentially with SF (see Tab. I), while also resulting in higher receiver sensitivity thus extending communication range and improving outage performance. Meanwhile, uplink transmissions must also satisfy an additional maximum $p_0 = 1\%$ duty cycling policy as specified by ETSI.

LoRa networks have a limited capacity and scalability [6] due to their low data rates and simple MAC scheme called

978-1-7281-5089-5/20/$31.00 ©2020 IEEE

LoRaWAN that essentially utilizes the ALOHA protocol with no collision avoidance provisions. LoRaWAN does however have provisions for an adaptive data rate (ADR) mechanism for optimizing the allocation of SFs with respect to the channel conditions. Basically, unless otherwise specified by the network operator, an ED will decide to use the ADR mechanism to adapt its SF according to the measured signal-to-noise (SNR) feedback [3]. More specifically, the allocated SF of each ED uplink transmission is set by the NS by sending a SNR link margin feedback in response to short test frames sent out by each ED after it successfully joins a network [11]. In this and many other works, the SFs are therefore assumed to be static and are allocated according to the distance between the EDs and their nearest GW, thus forming a kind of tiered ring structure around each GW (see Fig. 1). The corresponding ranges for each SF tier (SF-ring) are symbolically represented in the last column on Tab. I and depend on the specifics of the wireless propagation environment. Other SF assignment schemes (e.g., random and area-proportional [4]) have been studied, at least for the single-cell LoRa system but to the best of our knowledge there have not been any real deployments of them yet nor have the effects of multi-cell deployments been considered.

GWs can receive signals from multiple end-devices simultaneously due to the orthogonality of transmission sub-bands and quasi-orthogonality of SFs. Individual collisions of signals of different SFs are practically orthogonal since the rejection gain ranges from 16 to 36 dB. This performance however degrades once cumulative interference effects begin to take effect resulting to a further coverage loss as reported by [8]. Nevertheless, LoRa systems benefit significantly from this pseudo-orthogonality between SFs allowing LoRa networks to scale and support significantly more EDs than many other technologies; a key requirement of any wireless IoT solution [2]. Notably, as seen in Tab. II, the aggregate signal-to-interference (SIR) ratio required for a successful uplink transmission is $w = 1\text{dB} = 1.259$ for co-SF collisions, while it is in the range of -8 to -25dB corresponding to a factor of 0.15 or 0.0032, respectively for non-co-SF collisions. Thus, interference from a non-co-SF transmission is less important to network performance by at least a factor of 10 compared to that from a co-SF uplink transmission. We will therefore ignore non-co-SF interference as it is a secondary effect.

Finally, each ED broadcast transmission may be received by any number of GWs [3], therefore offering a kind of distributed spatial diversity gain. The GWs then forward their decoded packets to the LoRa NS, through a backhaul link (either cellular, Ethernet, satellite, or Wi-Fi), that manages the network and as part of its function it acts to eliminate duplicate any packets, performs security chesks, schedules acknowledgements through the optimal GW, and adapts data rates [3]. This spatial diversity offered by multi-cell LoRa networks has to the best of our knowledge not been studied analytically before.

III. Multi Gateway: Uplink System Model

A. Spatial Distribution of GWs and EDs

We assume that GWs and EDs are uniformly and randomly located in $\mathbb{R}^2$ space described by the homogeneous PPPs Φ_{GW} and Φ_{ED}, with constant intensity functions λ_{GW} and λ_{ED}, respectively; typically, $\lambda_{\text{GW}} \ll \lambda_{\text{ED}}$. Each point $\mathbf{x}_i$ and $\mathbf{y}_j$ of the PPPs represents an ED and a GW, respectively. Moreover, we let ED $i = 0$ be located at the origin of the coordinate system (i.e., $\mathbf{x}_0 = \mathbf{0}$) and $d_{ij} = |\mathbf{x}_i - \mathbf{y}_j|$ represent the Euclidean distance in km from ED $i = 0, 1, 2, \ldots$ to GW $j = 0, 1, 2, \ldots$. For notational convenience we assume that $d_{00} \leq d_{0j}$ for all $j > 0$, i.e., that GW $j = 0$ is the closest GW to ED $i = 0$. Also, note that the distance r to the k^{th} nearest GW is distributed according to $f_k(r) = \frac{2(\pi\lambda_{\text{GW}})^k}{(k-1)!} r^{2k-1} e^{-\lambda_{\text{GW}}\pi r^2}$ [12] while the typical distance between adjacent GWs is $1/\sqrt{\lambda_{\text{GW}}}$.

TABLE I
LoRa Characteristics of a 25 byte Message at BW = 125 kHz

SF	bit-rate kb/s	Packet air-time ms	Tx / h	Receiver Sens.	SNR q_{SF} dBm	Range km
7	5.47	36.6	98	-123 dBm	-6	$l_0 - l_1$
8	3.13	64	56	-126	-9	$l_1 - l_2$
9	1.76	113	31	-129	-12	$l_2 - l_3$
10	0.98	204	17	-132	-15	$l_3 - l_4$
11	0.54	372	9	-134.5	-17.5	$l_4 - l_5$
12	0.29	682	5	-137	-20	$l_5 - l_6$

TABLE II
SIR Collisions Thresholds in dB Between Different SFs [5]

SF	7	8	9	10	11	12
7	1	-8	-9	-9	-9	-9
8	-11	1	-11	-12	-13	-13
9	-15	-13	1	-13	-14	-15
10	-19	-18	-17	1	-17	-18
11	-22	-22	-21	-20	1	-20
12	-25	-25	-25	-24	-23	1

B. Rayleigh Channel Fading Model

We assume a block flat-fading channel h (quasi-static) modelled as a zero-mean, independent, circularly-symmetric complex Gaussian random variable with unit variance (i.e., Rayleigh fading) such that the channel gain $|h_{ij}|^2$ between ED i and GW j is modelled by an exponential random variable of mean 1. The effects of lognormal shadowing are not included in our model, suffice to say that such large-scale fluctuations of the signal are not expected to significantly affect our qualitative analysis. Further, we assume white Gaussian noise (AWGN) with zero-mean and variance $\mathcal{N} = -174 + \text{NF} + 10\log\text{BW}$ dBm, where NF is the receiver noise figure and is fixed for a given hardware implementation, here taken to be 6 dBm. For simplicity, we assume that uplinks use only a single BW= 125 kHz channel and a 25 Byte packet as described by Tab. I. All end-devices are assumed to transmit with a constant power $\mathcal{P} = 19$ dBm. A detailed discussions on transmission parameters can be found here [10].

C. Path Loss Attenuation

The coverage and capacity of wireless networks strongly depends on the behaviour of the attenuation function. While more accurate models do exist, for the sake of mathematical tractability we assume that the transmitted signal experiences

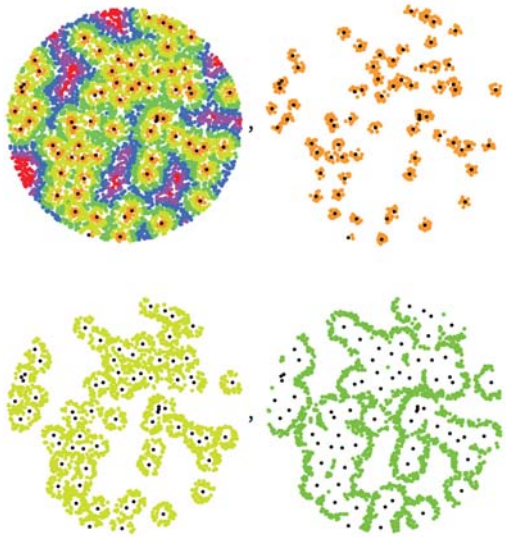

Fig. 2. Representation of two PPPs with $\lambda_{\mathrm{GW}} = 0.05$ and $\lambda_{\mathrm{ED}} = 5$ deployed in a circular region of radius $R = 20$ km. The GWs are the black points, while the EDs are coloured according to their distance to their nearest GW, and therefore their assigned SF. Sub-figures 2-4 show only the EDs in SFs 7, 8, and 9. Note that at areas of high concentrations of GWs, higher SFs (blue,purple, and red) essentially absent. Also, notice that the union of any SF colouring is a highly irregular region.

a path loss attenuation characterised by the function $g(d_{ij}) = \left(\frac{\lambda}{4\pi d_{ij}}\right)^{\eta}$ which follows from the Friis transmission equation, where $\lambda = 34.5$ cm is the carrier wavelength, and $\eta \geq 2$ is the path loss exponent usually taken to be equal to (2.7) 4 in (sub-) urban environments. We also assume isotropically radiating antennas at both transmitter and receiver ends and have assumed negligible interfering signals from non-LoRa signals operating in ISM frequencies.

D. SF Assignment of Uplink Transmissions

Spreading factors are typically set by the NS by sending SNR link margin feedback in response to short test frames sent out by end-devices after it successfully joins a network [3]. We will therefore assume that each ED will transmit with a SF dictated by the distance to its nearest GW according to Tab. I. For example, if $d_{00} \in (l_2, l_3]$, then ED $i = 0$ will transmit with $\mathrm{SF}_0 = 9$, and if $d_{00} \in (l_5, l_6]$, then ED $i = 0$ will transmit with $\mathrm{SF}_0 = 12$. This results in a tiered ring structure as seen in Fig. 2. Note that when two adjacent GWs are closer than $2l_i$ the rings merge to form figure eight regions. This a unique feature of LoRa networks that effectively dictates tiers of inhomogeneous PPPs wherein EDs contribute to co-SF interference.

E. Multi-Cell Spatial Diversity

According to Semech [3], each uplink transmission by an ED can be captured and decoded by multiple GWs if certain SNR and SIR requirements are met (these are presented in the following subsections). Importantly however LoRa GW do not apply multi-antenna cooperative decoding schemes such as maximum ratio combining (MRC) or zero-forcing. Instead, each LoRa GW that meets the SNR and SIR requirements will attempt to decode the ED transmission locally and independently before forwarding its decoded packets to the NS, where duplicate transmissions are filtered and removed [3]. An uplink transmission is thus said to be successful if it is successfully received by at least one GW. This simplified uplink diversity scheme found in LoRa networks is therefore not like most other schemes employed by distributed antennas systems (DAS) [13] and instead offers a non-standard gain to the success probability of an uplink transmission that we describe in (1).

F. Interference

LoRa chirp signals with different SFs are quasi-orthogonal (see Tab. II). Indeed, while this technology does create an extra set of "virtual" channels thus increasing the capacity of each GW, transmissions of similar spread remain susceptible to co-spreading factor interference. Due to the different sensitivities of each SF, EDs with similar SF will thus form tiers that resemble concentric rings (or doughnuts) around each GW node as seen Fig. 2.

In a single-cell setting, co-SF uplink interference therefore originates from EDs located in the same spatial tier/ring and scales like $\lambda_{\mathrm{ED}}\pi(l_{k-6}^2 - l_{k-7}^2)$ for $k \in [7, 12]$. Thus, the number of interferes in a single-cell LoRa system grows quadratically with higher SFs.

In a multi-cell LoRa GW system, this picture is somewhat different as highlighted in Figs. 1 and 2. For example, co-SF interference may originate from EDs outside of the tier/ring of a specific GW, thus increasing the total number of interferers almost linearly with the number of GWs $\sim \lambda_{\mathrm{GW}}\lambda_{\mathrm{ED}}$. This growth in the number of interferes however exhibits diminishing returns and becomes sub-linear for large $\lambda_{\mathrm{GW}} \gg 1$ since tiers/rings of adjacent GWs begin to overlap and eventually vanish at higher SF tiers; EDs are almost always close enough to a GW to use lower SF transmissions (see dense clustering parts of Fig. 2). Moreover, the region from which co-SF interference originates becomes a highly irregular region, making any attempt to mathematically quantify interference non-trivial. We overcome this difficulty in the next section using heuristic approximations that are supported by numerical simulations in the Appendix.

G. SNR and SIR Requirements

Unlike other communications systems, e.g., cellular, where interference is treated as shot-noise and performance is measured by the signal-to-interference-plus-noise (SINR) condition [12], LoRa uplink transmissions have a dual requirement that separates SNR and SIR [6], [9], [11] Specifically, we say that an uplink transmission by ED i is successful if the following condition is met

$$\bigcup_{j} \left\{ \left(\mathrm{SNR}_{ij} \geq q_{\mathrm{SF}_i} \right) \bigcap \left(\mathrm{SIR}_{ij} \geq w \right) \right\}, \tag{1}$$

where we define the SNR between ED i and GW j as

$$\mathrm{SNR}_{ij} = \frac{\mathcal{P}|h_{ij}|^2 g(d_{ij})}{\mathcal{N}}, \tag{2}$$

and the SIR between ED i and GW j as

$$\mathrm{SIR}_{ij} = \frac{\mathcal{P}|h_{ij}|^2 g(d_{ij})}{\mathcal{I}_j}, \tag{3}$$

where $\mathcal{I}_j = \sum_{k \neq i} \chi_{ik} \mathcal{P}|h_{kj}|^2 g(d_{kj})$ is the total co-SF interference at j, with $\chi_{ik} = 1$ if ED k is transmitting with the

same SF as ED i, and zero otherwise. Equation (1) essentially captures the joint SNR and SIR decoding requirement at GW j, and the uplink spatial diversity offered by the NS when managing a multi-cell LoRa network. Therefore, the success probability of an uplink transmission by ED i is given by

$$H(\mathbf{x}_i) = \mathbb{P}\Big[\bigcup_j \Big\{\Big(\text{SNR}_{ij} \geq q_{\text{SF}_i}\Big) \bigcap \Big(\text{SIR}_{ij} \geq w\Big)\Big\}\Big]. \quad (4)$$

In the following section, we will unpack (4) into smaller components that are mathematically tractable and amenable to engineering analysis using models and definitions introduced in this section and tools from stochastic geometry [12].

IV. Mathematical Analysis

To make progress we shall first make use of the homogeneity and stationarity of the PPP and focus on ED $i = 0$. We then notice that the probability of an uplink transmission to be successfully decoded by at least one GW is equal to the complement probability of it not being decoded by any GW. Equation (4) can thus be rewritten as follows

$$H(\mathbf{x}_0) = 1 - \mathbb{P}\Big[\bigcap_j \overline{\Big(Q_{0j} \bigcap J_{0j}\Big)}\Big] \geq 1 - \prod_j \Big(1 - \mathbb{P}\left[Q_{0j}\right]\mathbb{P}\left[J_{0j}\right]\Big) \quad (5)$$

where we defined the events $Q_{ij} = (\text{SNR}_{ij} \geq q_{\text{SF}_i})$ and $J_{ij} = (\text{SIR}_{ij} \geq w)$, and assumed independence between these events, thus resulting in the lower bound probability inequality (see [7] eq. (5)). We have thus managed to simplify (4) into the product of the probabilities, $\mathbb{P}\left[Q_{0j}\right] = \mathbb{P}\left[\text{SNR}_{0j} \geq q_{\text{SF}_0}\right]$ and $\mathbb{P}\left[J_{0j}\right] = \mathbb{P}\left[\text{SIR}_{0j} \geq w\right]$, which we now turn our attention to.

A. SNR Analysis

Following from the definition of SNR in equation (2) we can immediately calculate

$$\mathbb{P}\left[\text{SNR}_{ij} \geq q_{\text{SF}_i}\right] = \mathbb{P}\left[|h_{ij}|^2 \geq \frac{\mathcal{N} q_{\text{SF}_i}}{\mathcal{P} g(d_{ij})}\right] = e^{-\frac{\mathcal{N} q_{\text{SF}_i}}{\mathcal{P} g(d_{ij})}}. \quad (6)$$

Notice that q_{SF_0} is essentially a piecewise function of d_{00}, such that $q_{\text{SF}_0}(d_{0j}) = 10^{\frac{-q_0}{10}}$ with $q_0 = \{6, 9, 12, 15, 17.5, 20\}$ if d_{00} falls in the corresponding distance range (see last column of Tab. I). This distance-dependent sensitivity of $q_{\text{SF}_0}(d_{00})$ results in equation (6) having a non-smooth, saw-tooth-like profile as originally proposed by the authors [6], and as shown in Fig. 3 that plots $e^{-\frac{\mathcal{N} q_{\text{SF}_0}}{\mathcal{P} g(d_{00})}}$ for $d_{00} \in (0, 8]$ km and compares it to numerical computer simulations.

All numerical simulations throughout this paper assume that $\eta = 3$ and $l_k = k$ km for $k \in [0, 5]$ and $l_6 = \infty$ km.

B. SIR Analysis

As previously discussed and shown in Fig. 2, the spatial distribution of co-SF interfering EDs is quite irregular, especially for large λ_{GW} when tiers/rings from adjacent GWs begin to overlap. Previous works have attempted to capture this effect for pairs of adjacent GWs that are not too close as to overlap [9]. Through close inspection of Fig. 2 we note that each set of EDs for different SFs resembles a Poisson cluster point process (PCPP) [12] where the GWs are the

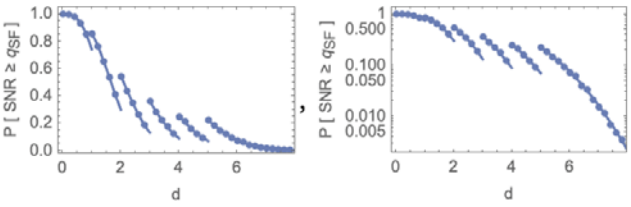

Fig. 3. Linear (left) and Log-linear (right) plot of the probability $\mathbb{P}\left[\text{SNR}_{00} \geq q_{\text{SF}_0}\right]$ vs. distance d_{00} between ED $i = 0$ and its nearest GW $j = 0$. The solid curved line is obtained analytically, while the dots represent numerical computer simulations.

parent and the EDs are the daughter points. Here however the daughter points in each SF-tier are often shared by parent GWs therefore deviating from classical cluster process, e.g., Matérn [12]. Moreover, despite this clustering observation, we note that the GW-ED pair distances are distributed according to the underlying PPPs Φ_{ED} and Φ_{GW} and thus postulate the PPP of EDs can be nicely partitioned into six (less dense) PPPs denoted here by $\Phi_{\text{ED}}^{(k)}$, for $k = 7, 8, \ldots 12$ with corresponding intensity functions $\lambda_{\text{ED}}^{(k)}$ such that $\Phi_{\text{ED}} = \bigcup_k \Phi_{\text{ED}}^{(k)}$ and $\lambda_{\text{ED}} = \sum_k \lambda_{\text{ED}}^{(k)}$. Specifically, we propose that each point in each sub-PPP $\Phi_{\text{ED}}^{(k)}$ represents an ED that transmits with SF=k. Moreover, we propose that the density $\lambda_{\text{ED}}^{(k)}$ of each of these sub-PPPs must somehow depend on λ_{GW} since at low GW-densities when there is no overlap between tier/rings we expect that $\lambda_{\text{ED}}^{(k)} \propto \lambda_{\text{GW}}(l_{k-6}^2 - l_{k-7}^2)$ for $k = 7, 8, \ldots 11$, but not for SF=12 since the last SF fills any remaining space and therefore behaves very differently. The dependence of $\lambda_{\text{ED}}^{(k)}$ on λ_{GW} is investigated in Appendix I, while arguments in favour of the Poissonarity of $\Phi_{\text{ED}}^{(k)}$ are presented in Appendix II.

Using the simplifying assumption of Poissonarity of the SF tiers, and following the definition of SIR in (3) we have

$$\begin{aligned}\mathbb{P}\left[\text{SIR}_{0j} \geq w\right] &= \mathbb{E}_{\mathcal{I}_j}\left[\mathbb{P}\left[|h_{0j}|^2 \geq \frac{w\mathcal{I}_j}{\mathcal{P} g(d_{0j})}\Big|\mathcal{I}_j\right]\right] \\ &= \mathbb{E}_{\mathcal{I}_j}\left[e^{-\frac{w\mathcal{I}_j}{\mathcal{P} g(d_{0j})}}\right] = \mathcal{L}_{\mathcal{I}_j}\left(\frac{w}{\mathcal{P} g(d_{0j})}\right),\end{aligned} \quad (7)$$

where $\mathcal{L}_{\mathcal{I}_j}$ is the Laplace transform of the random variable $\mathcal{I}_j$ evaluated at $\frac{w}{\mathcal{P} g(d_{0j})}$ conditioned on the locations of the ED at $\mathbf{x}_0$ and the GW at $\mathbf{y}_j$, and more specifically d_{0j}. Expanding the Laplace transform gives

$$\begin{aligned}\mathcal{L}_{\mathcal{I}_j}\left(\frac{w}{\mathcal{P} g(d_{0j})}\right) &= \mathbb{E}_{|h_{kj}|^2, d_{kj}}\left[e^{-\frac{w}{g(d_{0j})}\sum_{k>0}\chi_{0k}|h_{kj}|^2 g(d_{kj})}\right] \\ = \mathbb{E}_{d_{kj}}\Big[\prod_{k\geq 1}\mathbb{E}_{|h_{kj}|^2}\Big[e^{-w\chi_{0k}|h_{kj}|^2\frac{d_{0j}^\eta}{d_{kj}^\eta}}\Big]\Big] &= \mathbb{E}_{d_{kj}}\Big[\prod_{k\geq 1}\frac{1}{1+w\chi_{0k}\frac{d_{0j}^\eta}{d_{kj}^\eta}}\Big]\end{aligned} \quad (8)$$

since the channel gains $|h_{kj}|^2$ were assumed independent exponential random variables and we used the fact that $\frac{g(a)}{g(b)} = (b/a)^\eta$ and $\mathbb{E}_{|h|^2}[e^{-x|h|^2}] = \int_0^\infty e^{-z(x+1)}\mathrm{d}z = \frac{1}{1+x}$. Now, assuming that the interfering signals with SF= k arriving at GW j originate from EDs that are spatially distributed according to a PPP Φ_{ED}^k with intensity $p\lambda_{\text{ED}}^{(k)}$ (see Appendix I and II and recall the $p = 1\%$ duty cycle policy by ETSI [11])

enables us to absorb the χ_{0k} term and use the probability generating functional (PGF) of an inhomogeneous PPP [12] $\mathbb{E}\Big[\prod_{\xi\in\Xi} f(\xi)\Big] = \exp\Big(-\int_{\mathbb{R}^2}(1-f(\xi))\lambda(\xi)\mathrm{d}\xi\Big)$ to arrive at a closed form expression for the Laplace transform

$$\mathcal{L}_{\mathcal{I}_j}\left(\frac{w}{\mathcal{P}g(d_{0j})}\right) = \exp\Big(-2\pi p\lambda_{\mathrm{ED}}^{(k)}\int_{l_{k-7}}^{\infty}\frac{w\frac{d_{0j}^{\eta}}{d_{kj}^{\eta}}}{1+w\frac{d_{0j}^{\eta}}{d_{kj}^{\eta}}}d_{kj}\mathrm{d}d_{kj}\Big)$$
$$= \exp\Big(-\frac{2\pi p\lambda_{\mathrm{ED}}^{(k)}wd_{0j}^{\eta}}{l_{k-7}^{\eta-2}(\eta-2)}F_{21}\big(\frac{wd_{0j}}{l_{k-7}^{\eta}}\big)\Big), \tag{9}$$

where we have defined $F_{21}(x) = {}_2F_1[1, 1-\frac{2}{\eta}, 2-\frac{2}{\eta}, -x]$ to save space; ${}_2F_1$ is the Gauss Hypergeometric function that can be easily calculated to machine precision. Note that for the special cases of $\eta = 2$ and $\eta = 4$, we have that $F_{21}(x) = {}_2F_1[1,-1,0,-x] = 1$ and $F_{21}(x) = {}_2F_1[1,0,1,-x] = \frac{1}{\sqrt{x}}\arctan\sqrt{x}$, respectively. Notice also that the lower limit of the integral in (9) is l_{k-7} since any ED transmitting with SF $= k$ cannot be closer than l_{k-7} to any GW by construction. Also, for $k = 7$, i.e. when $d_{00} \le l_1$, equation (9) further simplifies to $\exp\big(-2\pi p\lambda_{\mathrm{ED}}^{(7)}\frac{w^{2/\eta}\pi d_{0j}^2}{\eta\sin\frac{2\pi}{\eta}}\big)$.

To verify the expressions obtained through our analysis and aforementioned assumptions, we numerically calculate using Monte Carlo computer simulations $\mathbb{P}[\mathrm{SIR}_{00} \ge w]$ as a function of d_{00}, using $w = 1$ dB $= 1.259$ (taken from the diagonal of Tab. II) and compare with the analytical expressions of (9). The results show very good agreement in Fig. 4. Observe that at low GW densities, an ED that is allocated a SF of 12 (i.e. is more than l_5 km from its nearest GW) has almost no chance for a successful transmission. This is because of the overwhelming number of co-SF interfering EDs (see right sub-figure of Fig. 4). This picture is completely reversed at high GW densities where the density of ED in higher SFs (red and purple lines in Fig. 4) is diminished.

C. Success Probability Analysis

Having calculated the two components that make up (5), $\mathbb{P}\left[\mathrm{SNR}_{0j} \ge q_{\mathrm{SF}_0}\right]$ and $\mathbb{P}\left[\mathrm{SIR}_{0j} \ge w\right]$, we are now left with calculating the product over all GWs j

$$H(\mathbf{x}_0) \ge 1 - \prod_j\big(1-\mathbb{P}\left[Q_{0j}\right]\mathbb{P}\left[J_{0j}\right]\big) = 1-\big(1-\mathbb{P}\left[Q_{00}\right]\mathbb{P}\left[J_{00}\right]\big)$$
$$\times\,\mathbb{E}_{d_{0j}}\Big[\prod_{j\ge1}\Big(1-\mathbb{P}\left[Q_{0j}|d_{0j}\right]\mathbb{P}\left[J_{0j}|d_{0j}\right]\Big)\Big]$$
$$= 1-\Big(1-e^{-\frac{\mathcal{N}q_{\mathrm{SF}_0}}{\mathcal{P}g(d_{00})}}\mathcal{L}_{\mathcal{I}_0}\Big(\frac{w}{\mathcal{P}g(d_{00})}\Big)\Big)$$
$$\times\,\exp\Big(-2\pi\lambda_{\mathrm{GW}}\int_{d_{00}}^{\infty}e^{-\frac{\mathcal{N}q_{\mathrm{SF}_0}}{\mathcal{P}g(x)}}\mathcal{L}_{\mathcal{I}_j}\Big(\frac{w}{\mathcal{P}g(x)}\Big)x\,\mathrm{d}x\Big), \tag{10}$$

where we have intentionally factorised out the $j = 0$ contribution to $H(\mathbf{x}_0)$ from all other GWs $j \ge 1$ since we are interested in understanding if a multi-cell LoRa network benefits (if any) from further densification. Namely, we may consider the penultimate line in (10) as the single-cell performance multiplied by the last line which captures the spatial diversity effect of LoRa networks.

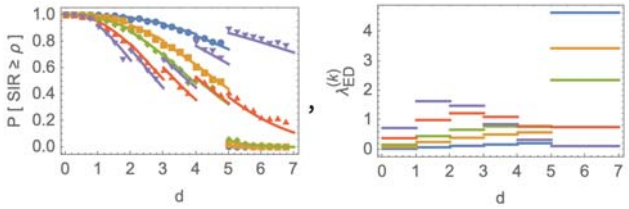

Fig. 4. The left plot shows numerical simulations of $\mathbb{P}[\mathrm{SIR}_{00} \ge w]$ as a function of d_{00} for $\lambda_{\mathrm{ED}} = 5$ EDs per km^2 and for different $\lambda_{\mathrm{GW}} = 0.001, 0.005, 0.01, 0.025, 0.05$ (blue, orange, green, red, purple) GWs per km^2. Solid curves are obtained analytically from (9). The right plot shows the corresponding values of $\lambda_{\mathrm{ED}}^{(k)}$.

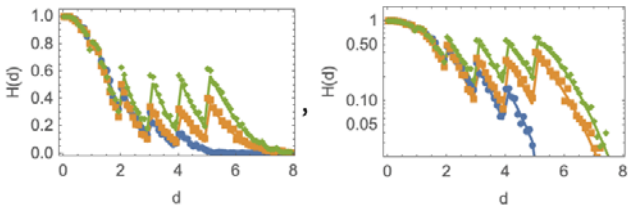

Fig. 5. Comparison of numerical simulations and the analytical derivation of (10) for the success probability $H(\mathbf{x}_0)$ as a function of d_{00} for $\lambda_{\mathrm{ED}} = 5$ and different values of $\lambda_{\mathrm{GW}} = 0.01, 0.05$ and 0.1 (blue, orange, green).

Unfortunately, the integral in the last line of (10) cannot be further simplified and has to be computed numerically. Fig. 5 plots $H(\mathbf{x}_0)$ as a function of d_{00} for different GW densities, demonstrating that GW densification of the networks does indeed benefit the success probability. Specifically, the benefits seem to be more noticeable at larger distances from the nearest GW and thus for higher SFs, since as discussed previously, larger SF tiers shrink in area (see Fig. 2) therefore reducing that co-SF interference in those tiers.

D. Coverage Probability

The coverage probability is the probability that a randomly selected ED is in coverage (i.e., not in outage) at any particular instance of time. One may obtain the system's coverage probability P^{cov} by deconditioning on the distance d_{00} between ED $i = 0$ and its nearest GW $j = 0$

$$P^{\mathrm{cov}}(\lambda_{\mathrm{ED}}, \lambda_{\mathrm{GW}}) = \int_0^{\infty} H(d_{00})f_1(d_{00})\mathrm{d}d_{00}, \tag{11}$$

where $f_1(r) = 2\pi\lambda_{\mathrm{GW}}re^{-\lambda_{\mathrm{GW}}\pi r^2}$ is the distance distribution of a randomly selected ED to its nearest GW.

Fig. 6 calculates and plots (11) for different values of ED and GW densities. It is observed that in order to provide adequate coverage in the uplink, the network operator must ensure that multiple GWs are deployed for denser and denser LoRa ED networks. Specifically, our analysis suggests that to ensure $\ge$80% coverage, the network operator must deploy GWs according to $\lambda_{\mathrm{GW}} \ge 0.013\lambda_{\mathrm{ED}}$, so about 1 GW for every 100 EDs.

V. Conclusion

We have mathematically investigated the effects of interference in a multi-cell LoRa network, a LPWA technology with promising IoT applications. Unlike other wireless networks, LoRaWAN employs an ADR CSS modulation

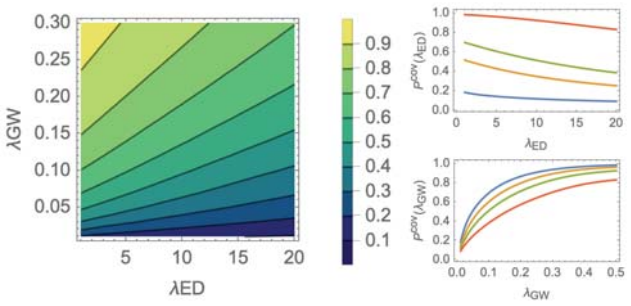

Fig. 6. Contour plot of the coverage probability $P^{\text{cov}}(\lambda_{\text{ED}}, \lambda_{\text{GW}})$ of a multi-cell LoRa network. The plots on the right are cross sections of the contour plot at $\lambda_{\text{GW}} = 0.01, 0.05, 0.1, 0.5$ and $\lambda_{\text{ED}} = 1, 5, 10, 20$ (blue, orange, green, red).

scheme, thus trading-off throughput for range while improving its susceptibility to wireless interference. Interference is however present at the GW nodes when uplink signals from EDs simultaneously collide in time, frequency, and SF. To mitigate this shortcoming, uplink transmissions can be received and decoded by multiple GWs, later to be filtered by the NS for any duplicate packets thus offering a kind of spatial diversity gain (SDG). These three features (ADR, co-SF interference, and multi-cell SDG) that are unique to LoRa networks have never been studied together before.

To that end, we have included these features in our system model and showed that LoRa networks spatially can be adequately modelled as appropriately thinned inhomogeneous PPPs. Further, leveraging tools from stochastic geometry we have obtained closed form expressions for various network properties such as the coverage probability and used this to analyse network performance as more GWs and EDs are added. We found that network densification tends to push EDs into the lower SF ADR tiers since higher SFs (with higher receiver sensitivities) become unoccupied and thus unutilized. While this increases co-SF interference in the lower SF tiers, GW densification has an overall positive effect on coverage enabling the network to scale while maintaining adequate coverage. Our analysis did not consider the effects of GW densification to network capacity, however this is expected to increase since lower SFs have a higher data rate and also lower time-on air, both of which are encouraging towards the use of LoRa in large scale IoT applications.

APPENDIX I

In Sec. IV-B it was postulated that the PPP of EDs Φ_{ED} can be nicely partitioned into six sub PPPs, each with corresponding intensities given by $\lambda_{\text{ED}}^{(k)}$ where $k \in [7, 12]$ is the SF of the uplink transmissions and $\lambda_{\text{ED}} = \sum_{k=7}^{12} \lambda_{\text{ED}}^{(k)}$. It therefore requires, that each point in $\Phi_{\text{ED}}^{(k)}$ represents an ED that transmits with SF=k, therefore implying that the closest GW to a point in $\Phi_{\text{ED}}^{(k)}$ must be $x \in (l_{k-7}, l_{k-6}]$ km away.

To make progress towards assessing this hypothesis, we numerically simulate Φ_{ED} and Φ_{GW} in a finite circular region of radius $R = 20$ km, at different intensities λ_{ED} and λ_{GW}, allocate SFs to EDs according to the distance to their nearest GW (as done in Fig. 2) and then count the total number of EDs $N_{\text{ED}}^{(k)}(\lambda_{\text{ED}}, \lambda_{\text{GW}})$ for SF tiers $k \in [7, 12]$.

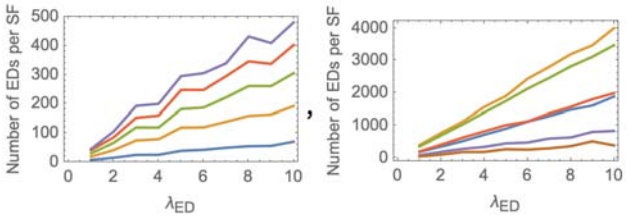

Fig. 7. Average number of EDs in each SF tier in a multi-cell LoRa network. The left plot corresponds to a sparse GW deployment with $\lambda_{\text{GW}} = 0.001$ GWs per km^2 whilst the right plot corresponds to a dense GW deployment with $\lambda_{\text{GW}} = 0.05$ GWs per km^2. In the left plot, the curve colors correspond (reading from the bottom) to blue-SF7, orange-SF8, green-SF9, red-SF10, purple-SF11, brown-SF12. Note that the brown curve corresponding to SF=12 tier is not shown in the left plot since it is way above the other 5 curves and linearly increases to $N_{\text{ED}}^{(12)} \approx 11500$ at $\lambda_{\text{ED}} = 10$ EDs per km^2. The colourings of the different tiers is the same on the right plot.

We first investigate the relationship of $N_{\text{ED}}^{(k)}(\lambda_{\text{ED}}, \lambda_{\text{GW}})$ with respect to λ_{ED}. Fig. 7 plots the number of EDs per SF as a function of λ_{ED} for different values of $\lambda_{\text{GW}} = 0.001$ (sparse GW deployment with typical distance between two adjacent GWs equal to $1/\sqrt{\lambda_{\text{GW}}} = 31.6$ km) and $\lambda_{\text{GW}} = 0.05$ (dense GW deployment with typical distance between two adjacent GWs equal to $1/\sqrt{\lambda_{\text{GW}}} = 4.5$ km)). Note that both plots exhibit a linear relationship with λ_{ED}, thus implying that $N_{\text{ED}}^{(k)}(\lambda_{\text{ED}}, \lambda_{\text{GW}}) \propto \lambda_{\text{ED}}$. Also note that for sparse GW deployments (e.g. $\lambda_{\text{GW}} = 0.001$), most EDs are allocated a SF of 12 since they are more than l_5 km away from their nearest GW. Indeed, we can expect that the average number of EDs in each tier in sparse GW deployments (minimal overlap between GWs) is given by

$$N_{\text{ED}}^{(k)}(\lambda_{\text{ED}}, \lambda_{\text{GW}} \ll 1) \approx (\lambda_{\text{GW}} \pi R^2) \times (\lambda_{\text{ED}} \pi (l_{k-6}^2 - l_{k-7}^2)), \tag{12}$$

for $k \in [7, 11]$ and by conservation of the total number of EDs we have that

$$N_{\text{ED}}^{(12)}(\lambda_{\text{ED}}, \lambda_{\text{GW}}) \approx (\lambda_{\text{ED}} \pi R^2) - \sum_{k=7}^{11} N_{\text{ED}}^{(k)}(\lambda_{\text{ED}}, \lambda_{\text{GW}}). \tag{13}$$

Approximation signs are used here since the left hand sides of (12) and (13) are integers. In (12), the first term is the average number of GWs while the second term is the average number of EDs in each ring/tier per GW. This equation does not hold for dense deployments where the tiers of adjacent GWs overlap, as can be seen in the right plot of Fig. 7 where the order of the six linear curves has been changed. Notably, the number of EDs with a SF of 12 now make up the smallest proportion of all EDs. We can therefore consider (12) as an approximation of $N_{\text{ED}}^{(k)}$ in a Taylor expansion near $N_{\text{GW}} \ll 1$

$$N_{\text{ED}}^{(k)} \approx \lambda_{\text{GW}} \pi R^2 \lambda_{\text{ED}} \pi (l_{k-6}^2 - l_{k-7}^2) \Big(1 + \mathcal{O}(\lambda_{\text{GW}})\Big). \tag{14}$$

We now investigate the relationship of $N_{\text{ED}}^{(k)}$ with respect to λ_{GW}. Having shown that $N_{\text{ED}}^{(k)} \propto \lambda_{\text{ED}}$, we choose $\lambda_{\text{ED}} = 2$ and plot in Fig. 8 the number of EDs per SF as a function of λ_{GW}, and numerically fit the data to curves of the form

$$g(\lambda_{\text{GW}}, \lambda_{\text{ED}}; v_k) = \lambda_{\text{GW}} \pi R^2 \lambda_{\text{ED}} \pi (l_{k-6}^2 - l_{k-7}^2) e^{-\pi v_k \lambda_{\text{GW}}}, \tag{15}$$

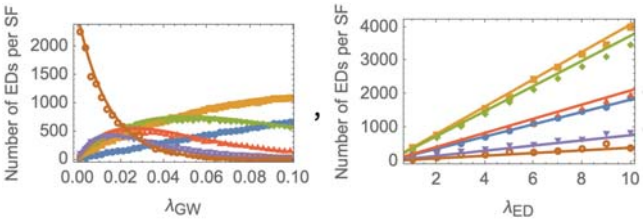

Fig. 8. Average number of EDs in each SF tier in a multi-cell LoRa network. The left plot corresponds to a sparse ED deployment with $\lambda_{\mathrm{ED}} = 2$ EDs per km^2 with varying GW deployment density. The points are obtained from numerical Monte Carlo simulations while the solid curves are plotted using (15) and the fitted values of v_k. The right plot is the same as the right plot from Fig. 7 showing how (15) completely characterises $N_{\mathrm{ED}}^{(12)}(\lambda_{\mathrm{ED}}, \lambda_{\mathrm{GW}})$. The colourings of the different SFs is as in Fig. 7.

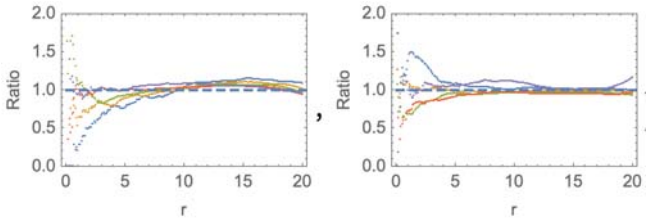

Fig. 9. The ratio of the numerically simulated Ripley function for the different SF tiers and the analytically calculated value for a PPP of density $\lambda_{\mathrm{ED}}^{(k)}$ deployed in a circular region of radius $R = 20$ km. The left plot takes as input $(\lambda_{\mathrm{ED}}, \lambda_{\mathrm{GW}}) = (5, 0.01)$ i.e. about 500 EDs per GW, while the right plot takes $(\lambda_{\mathrm{ED}}, \lambda_{\mathrm{GW}}) = (10, 0.05)$ i.e. about 200 EDs per GW. Both plots converge to 1, thus demonstrating that despite the particularities of the SF allocation scheme of LoRaWAN (see Sec. III-D and [3]) the resulting point processes exhibit Poisson-like properties.

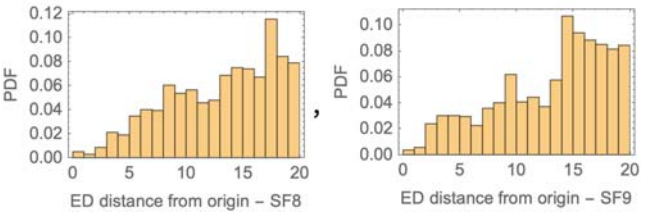

Fig. 10. Probability density function of the distance to the coordinate origin of all EDs in SF 8 (left) and SF 9 (right). Data is taken from Fig. 2. Notice that these demonstrate an almost linear behaviour with r.

where v_k is the parameter set to be fitted. The ansatz used in (15) was chosen since it meets the requirement of $e^{-\pi v_k \lambda_{\mathrm{GW}}} = 1 + \mathcal{O}(\lambda_{\mathrm{GW}})$, decays exponentially with λ_{GW} thus capturing how the regions of different SFs tend to shrink at higher GW densities due to overlapping tier/rings, and also it nicely fits our simulated data. Note that it is equivalent to fit straight lines with gradient v_k to the transformed data $-\ln \frac{N_{\mathrm{ED}}^{(k)}}{\lambda_{\mathrm{GW}}}$. A simple linear regression model is therefore used to obtain the values of $v_k = 0.51, 2.34, 6.22, 11.85, 19.57$.

Appendix II

The analysis in Appendix I has shown that the expected number of EDs in a PPP LoRa deployment in a finite circular region of radius R is given by

$$N_{\mathrm{ED}}^{(k)}(\lambda_{\mathrm{ED}}, \lambda_{\mathrm{GW}}) \approx g(\lambda_{\mathrm{GW}}, \lambda_{\mathrm{ED}}; v_k), \tag{16}$$

for $k \in [7, 11]$ using $v_k = 0.51, 2.34, 6.22, 11.85, 19.57$, and (13) for $k = 12$. In this section we provide arguments in favour of the Poissonarity of $\Phi_{\mathrm{ED}}^{(k)}$ by studying the spatial distribution of the $N_{\mathrm{ED}}^{(12)}(\lambda_{\mathrm{ED}}, \lambda_{\mathrm{GW}})$ EDs within each SF tier for different LoRa deployments by using the above results.

To do so, we have numerically calculated the number of ED points $\mathbf{x}_i$ that satisfy $\|\mathbf{x}_i\| \leq r$ and that belong to different SF tiers, and using the v_k obtained above we divide that with $\lambda_{\mathrm{ED}}^{(k)} K(r)$ where we have defined $\lambda_{\mathrm{ED}}^{(k)} \approx N_{\mathrm{ED}}^{(k)}(\lambda_{\mathrm{ED}}, \lambda_{\mathrm{GW}})/(\pi R^2)$ and $K(r) = \pi r^2$ is Ripley's function [12] for a PPP. As seen from Fig. 9, the ratio quickly approaches 1 after some initial fluctuations for all six SFs.

As second, similar argument in favour of the Poissonarity of $\Phi_{\mathrm{ED}}^{(k)}$ can be constructed by looking at the distance distribution of EDs from a GW. This is essentially the derivative of Ripley's function which for a PPP is linear in r. Fig. 10 plots the pdf of the distances for SFs 8 and 9 corresponding to the network deployments shown in Fig. 2.

The results presented in the Appendix do not claim that $\Phi_{\mathrm{ED}}^{(k)}$ are PPPs but offer some evidence of resemblance to a PPP at least in terms of the pair distance distribution. Such an approach has often been used in other works, e.g., to measure the Poissonarity of base stations in cellular networks [14].

VI. Acknowledgements

The authors would like to acknowledge funding from the EUs H2020 research and innovation programme under the Marie Skłodowska-Curie project NEWSENs, No 787180, and the EU Regional Development Fund and the Republic of Cyprus through the Research and Innovation Foundation, under the project INFRASTRUCTURES/1216/0017 (IRIDA).

References

[1] S. Madakam, *et al.*, "Internet of things (IoT): A literature review," *Journal of Computer and Communications*, vol. 3, p. 164, 2015.
[2] U. Raza, *et al.*, "Low power wide area networks: An overview," *IEEE Communications Surveys & Tutorials*, vol. 19, pp. 855–873, 2017.
[3] "What is LoRaWAN - LoRa Alliance," https://lora-alliance.org/sites/default/files/2018-04/what-is-lorawan.pdf.
[4] G. Zhu, *et al.*, "Improving the capacity of a mesh LoRa network by spreading-factor-based network clustering," *IEEE Access*, vol. 7, pp. 21 584–21 596, 2019.
[5] D. Croce, *et al.*, "Impact of LoRa imperfect orthogonality: Analysis of link-level performance," *IEEE Communications Letters*, vol. 22, no. 4, pp. 796–799, 2018.
[6] O. Georgiou and U. Raza, "Low power wide area network analysis: Can LoRa scale?" *IEEE Wireless Communications Letters*, vol. 6, no. 2, pp. 162–165, 2017.
[7] J.-T. Lim and Y. Han, "Spreading factor allocation for massive connectivity in LoRa systems," *IEEE Communications Letters*, vol. 22, no. 4, pp. 800–803, 2018.
[8] A. Mahmood, *et al.*, "Scalability analysis of a LoRa network under imperfect orthogonality," *IEEE Transactions on Industrial Informatics*, vol. 15, no. 3, pp. 1425–1436, 2018.
[9] L. Beltramelli, *et al.*, "Interference modelling in a multi-cell LoRa system," in *Wireless and Mobile Computing, Networking and Communications (WiMob)*, 2018, pp. 1–8.
[10] M. Bor and U. Roedig, "LoRa transmission parameter selection," in *2017 13th International Conference on Distributed Computing in Sensor Systems (DCOSS)*. IEEE, 2017, pp. 27–34.
[11] N. Sornin, *et al.*, "LoRaWAN Specifications," *LoRa Alliance*, 2015.
[12] M. Haenggi, *Stochastic geometry for wireless networks*. Cambridge University Press, 2012.
[13] J. Zhang and J. G. Andrews, "Distributed antenna systems with randomness," *IEEE Transactions on Wireless Communications*, vol. 7, no. 9, pp. 3636–3646, 2008.
[14] A. Guo and M. Haenggi, "Spatial stochastic models and metrics for the structure of base stations in cellular networks," *IEEE Transactions on Wireless Communications*, vol. 12, no. 11, pp. 5800–5812, 2013.